Energetics of titanium nitrides of composition Ti_2N

1998 J. Phys.: Condens. Matter 10 10223

(http://iopscience.iop.org/0953-8984/10/45/010)

J. Phys.: Condens. Matter **10** (1998) 10223–10240. Printed in the UK PII: S0953-8984(98)95060-3

Energetics of titanium nitrides of composition Ti_2N

R Eibler

Institute of Physical Chemistry, University of Vienna, Währingerstraße 42, A-1090 Wien, Austria

Received 12 June 1998

Abstract. The band structure and energetics of ϵ-Ti_2N and δ'-Ti_2N were calculated by means of the full-potential linearized augmented-plane-wave (FLAPW) method. In accordance with experiment, ϵ-Ti_2N was found to be more stable than δ'-Ti_2N. The transformation energy at 0 K was calculated as 9.35 kJ mol^{-1}. Relaxation of the Ti atoms stabilizes the δ'-phase and the relaxation energy of 28.75 kJ mol^{-1} is rather high.

A comparison with a former LAPW band-structure calculation that used a muffin-tin potential shows significant differences which are ascribed to the sensitivity of some very delocalized valence states to the approximations for the potential in the interstitial region. Thus, the importance of using a full potential for these compounds is stressed.

A FLAPW calculation for the fictitious compound δ'-Ti_2C furnishes qualitative explanations for the instability of the δ'-Ti_2N structure for this substance.

1. Introduction

Owing to its hardness and high stability, titanium nitride has found many applications in industry. It is used, for example, as a surface coating on cutting tools, and as a constituent in cemented carbides and in hardened steels [1, 2]. Some authors have tried to relate the hardness of specific titanium nitride samples to their phase composition [3, 4]. The study of the different phases occurring in the phase diagram of the Ti–N system is, therefore, interesting not only from the academic point of view [1, 2, 5].

TiN_x crystallizes in the cubic sodium chloride structure (δ-phase) over a wide range of composition, $0.42 \leqslant x \leqslant 1.02$, with the vacancies statistically distributed on the N sublattice [6]. The ranges of concentration of the δ-phase given by other authors [3, 5] differ slightly. For compositions with $0.5 \leqslant x \leqslant 0.6$, a long-range-ordered tetragonal defect structure of nominal composition Ti_2N, so-called δ'-Ti_2N, is obtained after annealing at 773 K [7–9]. Its unit cell, shown in figure 1, can be derived from two fcc unit cells on top of each other where the vacancies on the N sublattice occupy fixed positions (ordered $TiN_{0.5}$). The δ'-Ti_2N structure is obtained from this ordered $TiN_{0.5}$ by a tetragonal distortion of the unit cell resulting in a c/a ratio of 2.112 64 instead of 2.0. Neutron diffraction shows that—contrary to the findings of some earlier experiments—the Ti atoms of δ'-Ti_2N are shifted in the z-direction by $\Delta = 0.123$ Å *away* from their positions in the NaCl structure towards the nearest N neighbours [9].

δ'-Ti_2N is, however, only metastable [1, 10, 11] and transforms by ageing into thermodynamically stable ϵ-Ti_2N which crystallizes in the tetragonal primitive antirutile structure [12]. Its unit cell is shown in figure 2. ϵ-Ti_2N can be directly obtained from disordered δ-TiN_x only at high temperatures, because the transition is kinetically hindered and a high activation energy must be provided to initiate it [13]. Its formation is favoured by the presence of α-Ti [1]. ϵ-Ti_2N is also formed from δ-TiN and ζ-Ti_4N_3 [1, 14].

0953-8984/98/4510223+18$19.50

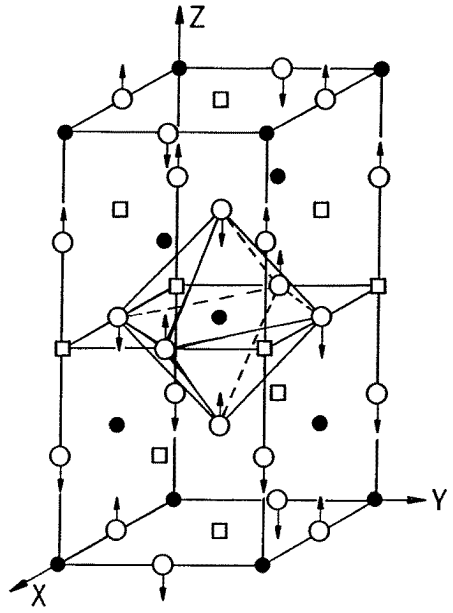

Figure 1. The tetragonal unit cell of δ'-Ti_2N. Full circles: N atoms; squares: N vacancies; empty circles: Ti atoms.

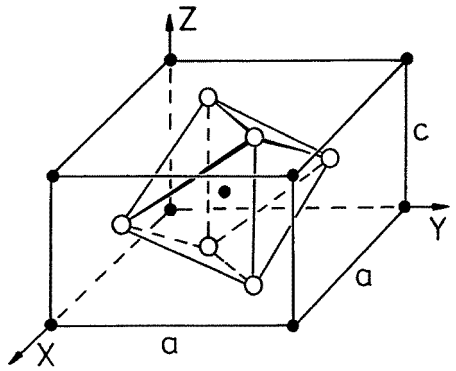

Figure 2. The unit cell of ϵ-Ti_2N. Full circles: N atoms; empty circles: Ti atoms.

In an earlier publication [15], the band structure, densities of states and electron densities of ϵ- and δ'-Ti_2N were calculated by means of the LAPW method [16, 17]. The chemical bonds were analysed and it was found that the relative stability of the two phases could be explained by qualitative arguments. For both the ϵ- and the δ'-phase, the Fermi level lies in, or near, a minimum of the density of states (DOS) whereas, for disordered δ-$TiN_{0.5}$, it is situated in the ascending part of the DOS d-band peak. In the two ordered structures the energies of the Ti t_{2g} states and—for ϵ-Ti_2N—also of the e_g states are lowered due to the formation of d–d σ-bonds. These states form one (two) subpeaks at the bottom of the DOS d band which are separated by the minimum mentioned above from the remainder of the peak. The formation of additional d–d bonds stabilizes the ordered phases with respect to the disordered phase.

However, for a quantitative discussion of the relative stabilities of δ'- and ϵ-Ti_2N, the total energies of both phases must be calculated. The accuracy of the LAPW method is not sufficient for this task. Therefore, the necessary calculations were performed by means of

the full-potential linearized augmented-plane-wave (FLAPW) method [18].

Recently, the DOS of ϵ-Ti_2N was calculated by Zhang *et al* [19] by means of the LMTO-ASA method. The authors claim good agreement with previous calculations [15, 20]. However, they locate the N p band of ϵ-Ti_2N at a 2 eV lower position than in [15] and separated by a gap of 2 eV from the Ti d band whereas, in the LAPW calculation [15], the p- and d-band overlap. Similar deviations exist between their DOS for δ-TiN and the DOS of δ-TiN from a previous APW band-structure calculation [20]. Thus, only the trends in the DOS on going from δ-TiN to ϵ-Ti_2N are well reproduced by their calculation.

2. Computational aspects

The FLAPW method is based on density functional theory [21] assuming the local density approximation (LDA). In our code, the Hedin–Lundqvist exchange potential [22] is used and the calculations are performed scalar relativistically for the valence states. The core states, including the so-called semi-core Ti 3s and 3p states, are treated as atomic-like and their energies are calculated fully relativistically. In the former LAPW calculation [15] the Ti 3s and 3p states were treated as semi-core band states and calculated in a separate energy window.

The FLAPW method makes use of a full potential without assuming the muffin-tin approximation inherent to the LAPW method. In the atomic spheres around the atomic positions (with radii R_{Ti} of 1.961 au and R_N of 1.732 au) the electron density and the potential are expanded in spherical harmonics up to $l = 8$. In the interstitial region between the atomic spheres the potential and the electron density are expanded in 8000–9000 plane waves corresponding to a maximum $\boldsymbol{K}$-vector of 4.6. The valence electron wave functions are expanded in 800–900 so-called augmented plane waves. The former LAPW band-structure calculations [15] used only basis sets of less than 500 augmented plane waves. In order to avoid ghost bands the energy parameters for the Ti s and p states are given fixed values of 1.0 and 2.5. All other energy parameters are determined from the centre of gravity of the l-like bands of the previous iteration.

As in [15], the tetrahedron method [23, 24] is used for the integrals in $\boldsymbol{k}$-space. The 18–20 non-equivalent $\boldsymbol{k}$-points which where used in [15] in order to obtain self-consistency do not suffice for energetic investigations because the total energies depend significantly on the number of $\boldsymbol{k}$-points in the mesh. Different $\boldsymbol{k}$-meshes must be used for tetragonal primitive ϵ-Ti_2N and for tetragonally centred δ'-Ti_2N with c/a ratios of 0.6118 and 2.112 64, respectively, in order to distribute the $\boldsymbol{k}$-points as evenly as possible in the respective irreducible wedges of the Brillouin zone. For results of comparable accuracy, the total energies should be extrapolated to an infinite number of $\boldsymbol{k}$-points.

For the geometry optimization, first the total energies for several volumes were calculated using different $\boldsymbol{k}$-meshes. The resulting energies were extrapolated to $\boldsymbol{k} \to \infty$. In this step, the c/a ratio, the internal parameter u for ϵ-Ti_2N and the Ti-atom relaxation Δ were frozen at the experimental values. The minimum of the total energy with respect to the volume and the corresponding equilibrium volume were determined by means of a Birch fit [25].

In a second step, equilibrium values for the c/a ratio, the internal parameter u and the relaxation Δ were found by energy minimization at a volume fixed at its equilibrium value and using comparable $\boldsymbol{k}$-meshes of 540 inequivalent $\boldsymbol{k}$-points for ϵ-Ti_2N and of 546 inequivalent $\boldsymbol{k}$-points for δ'-Ti_2N. The experimental lattice parameters and atomic positions are the same as in [15].

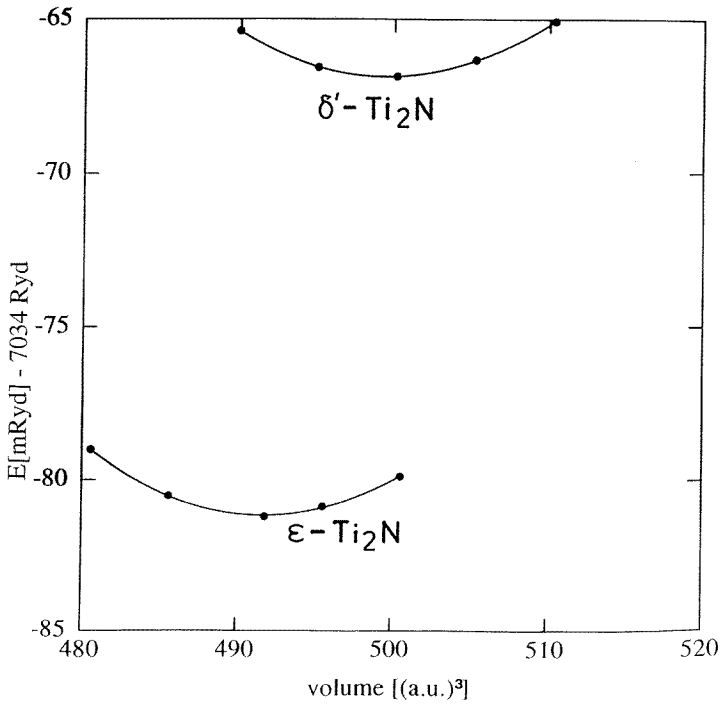

Figure 3. The volume dependence of the total energy/unit cell of ϵ-Ti_2N (lower curve) and of δ'-Ti_2N (upper curve).

3. Results

3.1. Energetics

Figure 3 shows Birch fits for the total energies of ϵ- and δ'-Ti_2N as functions of the volume. For both compounds, the equilibrium volume is about 2% lower than the volume found by experiment. This deviation is caused by the local density approximation inherent to the FLAPW code which overestimates the cohesion in solids. The total-energy curve of the ϵ-phase lies below the curve for the δ'-phase in accordance with the fact that ϵ-Ti_2N is found by experiment to be the thermodynamically stable phase. The ϵ-phase is stable at a 2% smaller volume than the δ'-phase which indicates the probability of stronger bonding in the former phase. The transformation energy (at 0 K) was calculated as 14.25 mRyd per unit cell (containing two formula units) corresponding to 2.25 kcal mol^{-1} or 9.35 kJ mol^{-1}, respectively. No experimental value for the δ'–ϵ transformation energy has been found in the literature but in [11] the transformation enthalpy $\Delta H_{\delta-\delta'}$ is given as 7.03 kJ mol^{-1} (64 J g^{-1}).

Band-structure methods such as the FLAPW method can only be applied to solids with translational symmetry. Therefore, we cannot calculate the total energy of disordered δ-$TiN_{0.5}$. We can, however, perform a band-structure calculation for ordered $TiN_{0.5}$ as described in the introduction, with a c/a ratio of 2.0 and with unrelaxed Ti atoms. The lattice constant for this fictitious structure is found by setting the volume of its unit cell equal to the equilibrium volume of the δ'-phase. The total energy of ordered $TiN_{0.5}$ is then 35 mRyd/unit cell (23 kJ mol^{-1}) higher than the total energy of the δ'-phase with

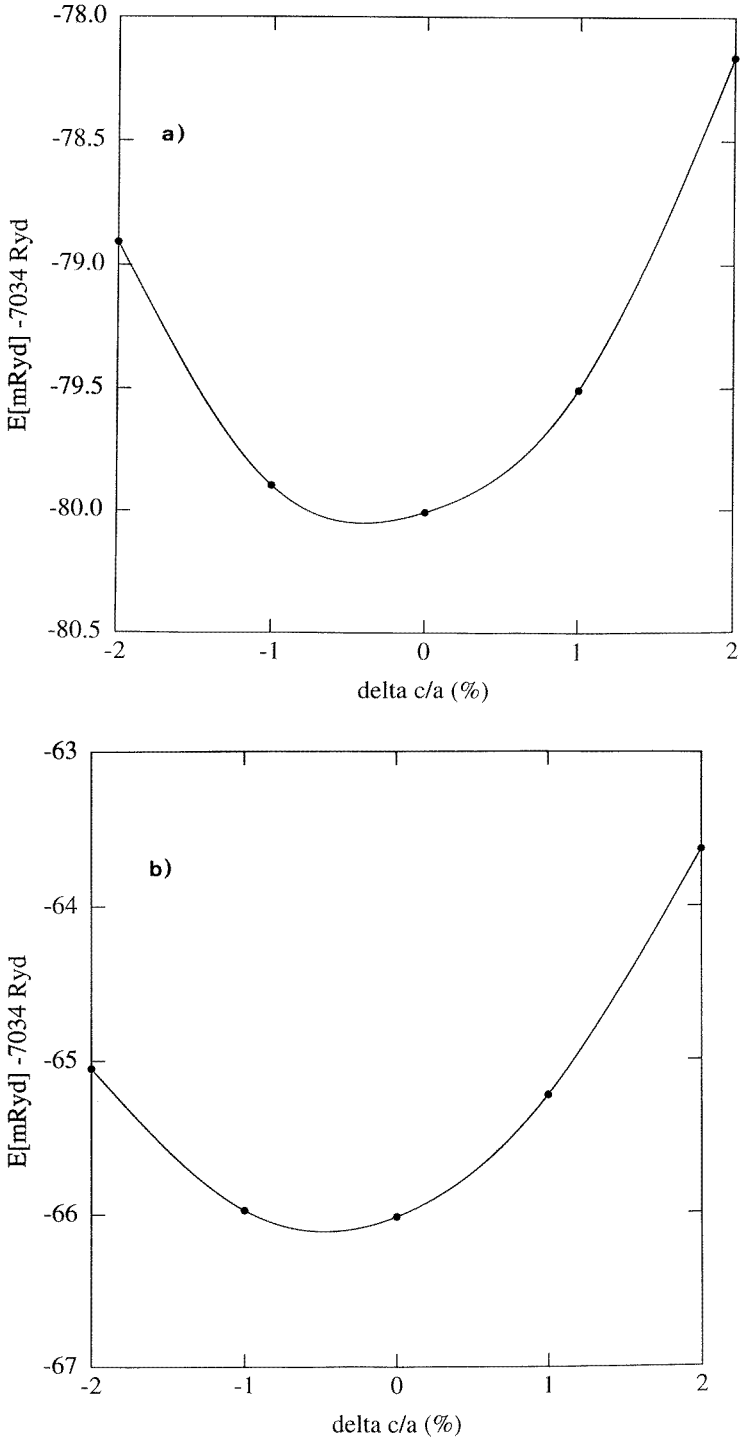

Figure 4. The variation of the total energy with the c/a ratio (as a percentage deviation from the experimental value) at the equilibrium volume for (a) ϵ-Ti_2N and (b) δ'-Ti_2N.

the same volume.

The equilibrium values for the other crystallographic parameters were determined by energy minimization at fixed equilibrium volume. Figure 4 shows the total energy as a function of the c/a ratio for (a) ϵ-Ti_2N and (b) δ'-Ti_2N. The deviation of the c/a ratios at the respective energy minima from the experimental values lies below -1% with an energy decrease of less than 0.05 mRyd/unit cell.

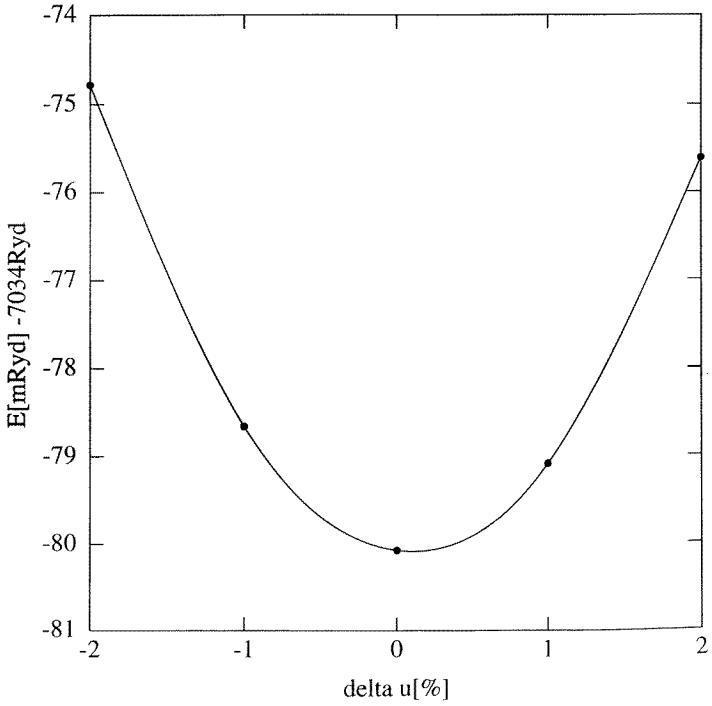

Figure 5. The total energy of ϵ-Ti_2N versus the internal parameter u determining the position of the titanium atoms in the unit cell.

The minimization of the total energy of ϵ-Ti_2N at the experimental c/a ratio with respect to the internal parameter u (figure 5) leads to an equilibrium u-value coinciding with the experimental value.

The influence of the relaxation of the Ti atoms on the total energy of δ'-Ti_2N (at the equilibrium volume and with the experimental c/a ratio) is shown by a solid curve in figure 6. The value of the Ti z-coordinate at the energy minimum lies at $0.141c$ (corresponding to 13% relaxation with respect to the unrelaxed position, of $0.125c$, which is assumed by the Ti atoms in the NaCl structure) instead of the experimental value of $0.139c$. The energy difference between the equilibrium and the experimental Ti relaxation is 1.1 mRyd/unit cell (0.7 kJ mol^{-1}) and the total relaxation energy—with respect to that of δ'-Ti_2N with unrelaxed Ti atoms—is calculated as 43.1 mRyd/unit cell (28.75 kJ mol^{-1}). Relaxation of the Ti atoms reduces the nearest-neighbour Ti–N distance in the z-direction by 13% and, therefore, the bond strength of the σ-bonds between the Ti d_{z^2} orbitals and the N s and p_z orbitals increases accordingly. A significantly lower total energy results.

If the Ti atoms in ordered $TiN_{0.5}$ with a c/a ratio of 2.0 are allowed to relax at constant volume, the total energy changes as shown by the dashed curve of figure 6. *Without relax-*

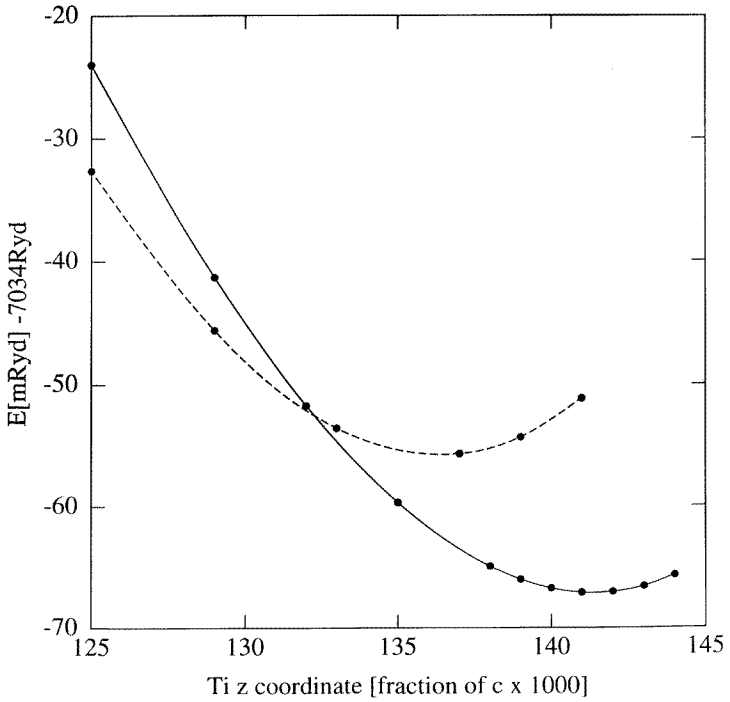

Figure 6. The total energy of δ'-Ti_2N versus the relaxation of Ti atoms in the z-direction given in fractions of the lattice parameter c multiplied by 1000. Solid curve: relaxation for the experimental c/a ratio of 2.112 64; dashed curve: relaxation for the ordered $TiN_{0.5}$ structure with $c/a = 2.0$

ation, the total energy of ordered $TiN_{0.5}$ lies 8.6 mRyd/unit cell below the energy of δ'-Ti_2N. If the Ti atoms are allowed to relax, though, the total energy of ordered $TiN_{0.5}$ decreases only by 23.09 mRyd/unit cell compared to 43.1 mRyd/unit cell in the case of of δ'-Ti_2N. Therefore, the δ'-Ti_2N structure is, for *relaxed* Ti atoms, more stable than the ordered $TiN_{0.5}$ structure.

3.2. Band structure and densities of states

Ample discussion of the LAPW band structures and densities of states of ϵ- and δ'-Ti_2N can be found in [15]. At this stage, therefore, only the differences between LAPW and FLAPW results will be discussed.

Figure 7 shows in panel (a) the FLAPW band structure of ϵ-Ti_2N for the equilibrium geometry and, in order to facilitate comparison, in panel (b) the corresponding LAPW band structure [15] for the experimental geometry. Deviations can be detected, for example near the centre of the Brillouin zone (point Γ). The eigenvalues with a large amount of charge in the interstitial region (e.g. the eighth and eleventh eigenvalues at Γ with 70% (80%) charge in the interstitial region) react sensitively to the change in the interstitial potential from a constant in the LAPW method to the Fourier expansion of the present FLAPW calculation and are shifted in the latter case by 0.1 (0.11) Ryd to higher energies. Other eigenvalues with more localized wave functions change their position much less or not at

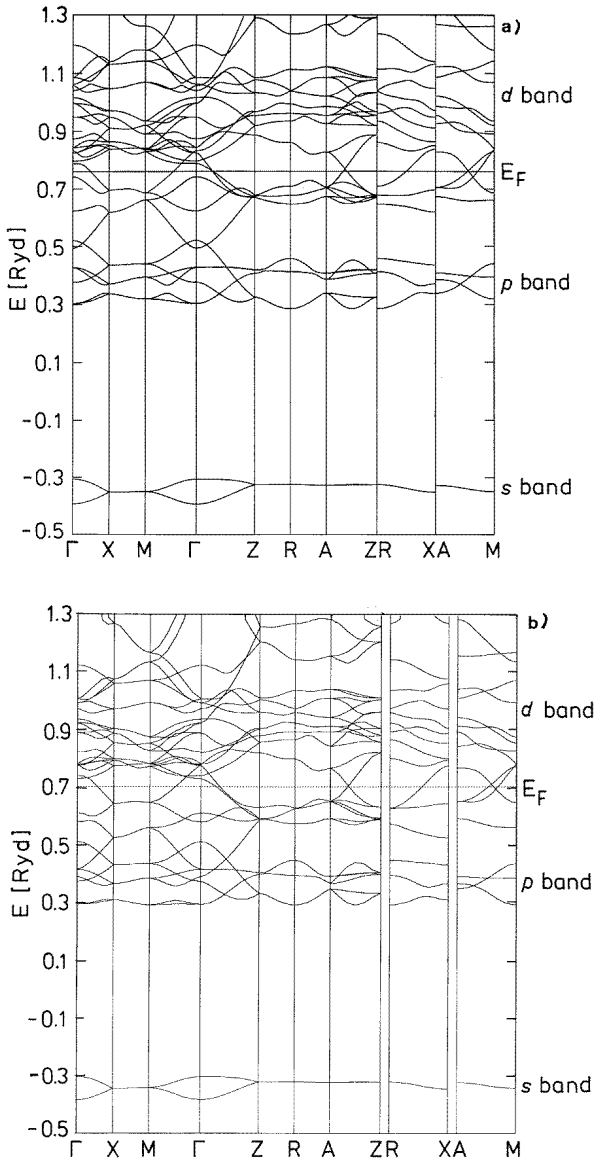

Figure 7. The band structures of ϵ-Ti_2N in some symmetry directions of $\boldsymbol{k}$-space. (a) The FLAPW band structure for the equilibrium geometry. (b) The LAPW band structure [15] for the experimental geometry.

all. The sequence of eigenvalues at Γ is, therefore, modified, leading to local differences in the LAPW and FLAPW band structures.

Figure 8 shows in panel (a) the FLAPW band structure of δ'-Ti_2N for the equilibrium geometry and, for comparison, in panel (b) a section of the LAPW band structure [15] of this compound for the experimental geometry. The deviations of the FLAPW from the LAPW energy bands near Γ are less pronounced than for ϵ-Ti_2N. However, the s and p bands are shifted to slightly lower energies and, whereas the p and d bands overlap at Γ in

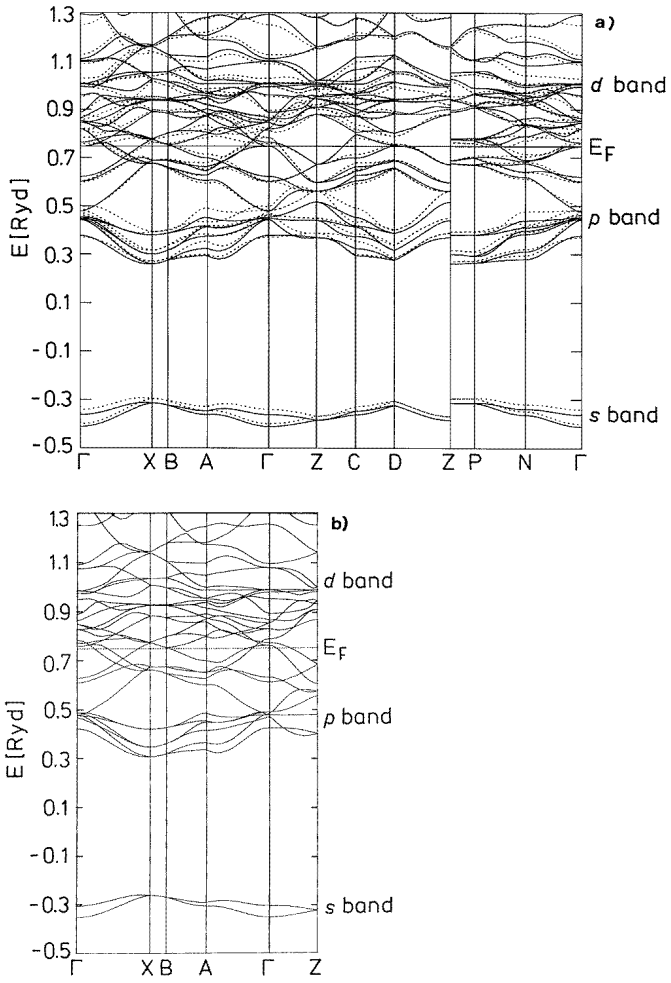

Figure 8. The band structures of δ'-Ti_2N in some symmetry directions of $\boldsymbol{k}$-space. (a) The FLAPW band structure for the equilibrium geometry for relaxed (full curve) and unrelaxed (dotted curve) Ti atoms. (b) A section of the LAPW band structure [15] for the experimental geometry.

the LAPW band structure, no overlap is found in the FLAPW case.

In order to show the influence of the relaxation of the Ti atoms on the band structure, the bands of the unrelaxed band structure of δ'-Ti_2N are also shown as dotted lines in figure 8(a). Without relaxation, the increased N–Ti distance in the z-direction leads to weaker Ti d_{z^2}–N (s, p_z) bonds. Therefore, the corresponding bonding states at the top of the s and p band are shifted to higher energies and the antibonding states at the top of the d band to lower energies. The p bandwidth increases accordingly and, as a consequence, the p and d bands overlap at Γ. The d-band states undergo variable shifts according to their individual charge distribution.

The differences between the LAPW and FLAPW band structures also give rise to differences in the corresponding densities of states. Figure 9 shows the FLAPW (solid curve) and LAPW (dotted curve) densities of states (DOS) of δ'-Ti_2N with the experimental

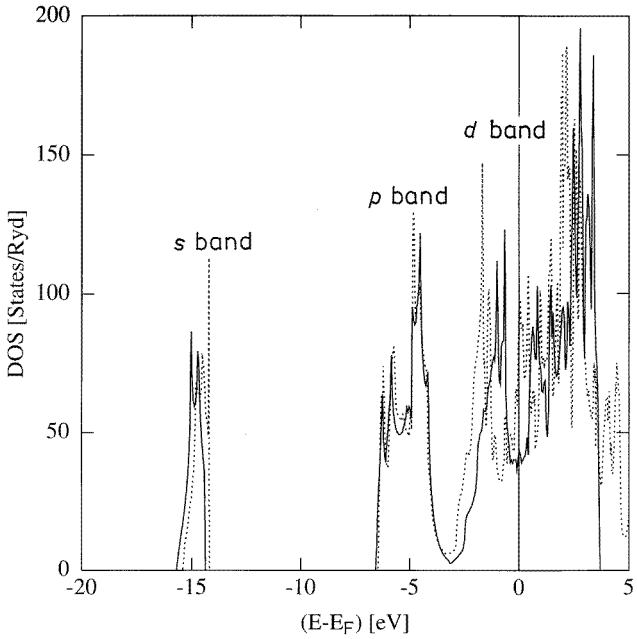

Figure 9. The FLAPW (solid curve) and LAPW (dotted curve) densities of states of δ'-Ti_2N with the experimental geometry in states of both spin directions per rydberg and per unit cell containing two formula units of Ti_2N.

geometry†. With respect to the LAPW DOS peak, the FLAPW DOS peak corresponding to the p band is shifted by 0.2 eV and the FLAPW DOS peak corresponding to the d band by 0.7 eV to higher energies. The FLAPW Fermi level lies exactly in the DOS minimum separating the lowest d-band peak from the rest of the d band. Also, the pseudogap between the p and d band is enlarged. The amount of d charge in the p band is reduced in the FLAPW calculation indicating less interaction between Ti d and N p states compared with that found from the LAPW calculation.

Figure 10 corresponds to figure 8 and shows the DOS of δ'-Ti_2N at the equilibrium geometry with (solid curve) and without (dotted curve) relaxation of the Ti atoms. The relaxation reduces the widths of all bands slightly and increases the pseudogap between p and d bands and also between occupied and unoccupied d-band states. The density of states at the Fermi level is reduced accordingly.

The DOS of unrelaxed δ'-Ti_2N and of unrelaxed ordered $TiN_{0.5}$ are almost indistinguishable apart from some slight differences in the relative peak heights.

Comparing the LAPW and FLAPW DOS of ϵ-Ti_2N with the experimental geometry (figure 11), some trends already observed for δ'-Ti_2N are even more pronounced: the p bandwidth and position remain relatively unchanged but the respective peak maxima are shifted to slightly higher energies. The most striking difference is a shift of the d band by 1.2 eV and of the Fermi level by 0.5 eV to higher energies. Also, instead of the distinct double-peak structure of the LAPW d band DOS below the Fermi energy, the FLAPW DOS in this energy region exhibits one peak with three maxima.

Thus, in the case of the two titanium nitrides, significant differences are found between

† In figures 9–12 the DOS curves are shifted in order to allow them to coincide at the bottom of the N s band.

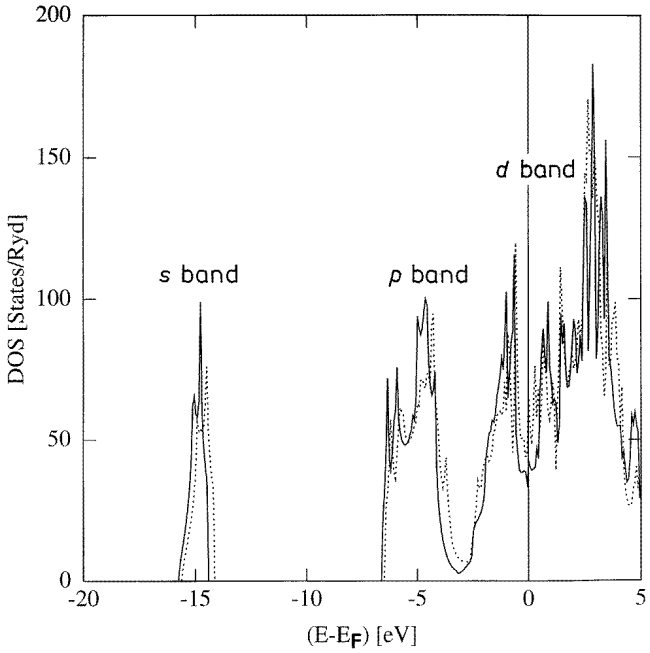

Figure 10. The FLAPW DOS of δ'-Ti_2N with (solid curve) and without (dotted curve) relaxation of the Ti atoms. For the DOS, the same units as in figure 7 are used.

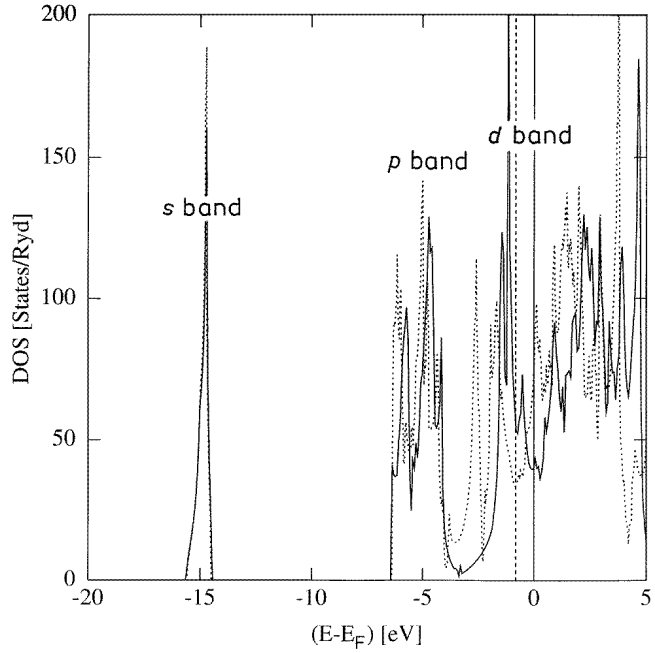

Figure 11. The FLAPW (solid curve) and LAPW (dotted curve) densities of states of ϵ-Ti_2N with the experimental geometry. For the DOS, the same units as in figure 7 are used.

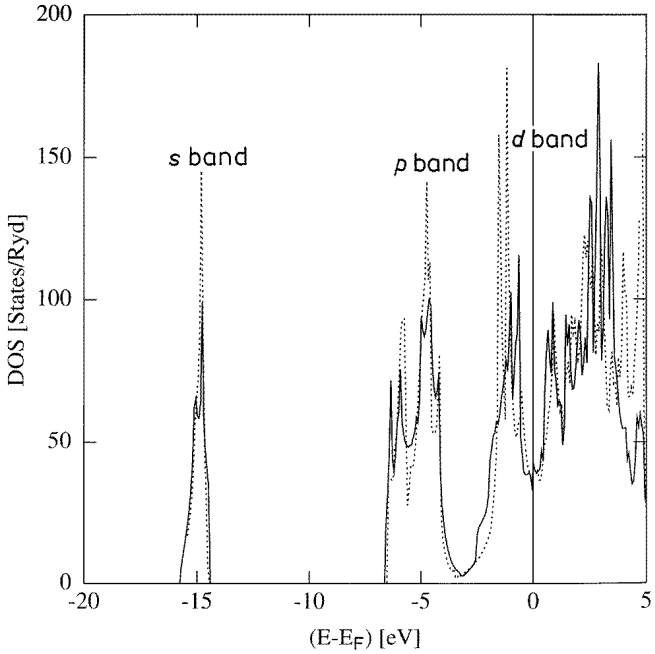

Figure 12. The FLAPW DOS of δ'-Ti_2N (solid curve) and that of ϵ-Ti_2N (dotted curve) for the equilibrium volumes. For the DOS, the same units as in figure 7 are used.

the LAPW and FLAPW band structures and densities of states. As already mentioned, some of the valence eigenstates have markedly delocalized wave functions and are thus extremely sensitive to differences in the interstitial potential. A similar effect was found for the highest occupied eigenstate of the semiconductor β-$FeSi_2$, with 54% charge outside the muffin-tin spheres. It was shown that ASW and LMTO-ASA band-structure calculations underestimate its energy by 0.4 eV with respect to full-potential band-structure calculations [26].

As regards a possible influence of the differences between the LAPW and FLAPW calculations in basis size and $\boldsymbol{k}$-mesh used for the Brillouin zone integrations, tests showed that the FLAPW band structures and densities of states did not change significantly if the same numbers of $\boldsymbol{k}$-points and basis functions as in the LAPW calculation were used. However, the total energies vary strongly with the numbers of $\boldsymbol{k}$-points and basis functions.

Also, a different treatment of the semi-core states—for example, calculating them in the same energy window as the valence states—did not change the DOS significantly.

If one compares the FLAPW DOS of δ'-Ti_2N (solid curve) and that of ϵ-Ti_2N (dotted curve) (figure 12), the main difference between the DOS of these two phases is a shift of the occupied d-band maximum of ϵ-Ti_2N by 0.8 eV to lower energies, indicating more efficient d–d bonding in the latter phase and thus furnishing an explanation for its higher stability. The positions of the s and p bands and the general shapes of the bands are roughly the same for the two phases and, for both of them, the Fermi level lies in a minimum of the DOS. However, the DOS peaks are slightly narrower for the ϵ-phase.

Recently, XPS spectra of substoichiometric titanium nitrides and carbonitrides were measured and the densities of states were calculated by means of the self-consistent tight-binding LMTO method [27]. The samples were prepared by implantation of N ions at the surface of pure titanium and consisted of cubic nanocrystallites with disordered vacancies

on the N sublattice sites. The calculations were performed for cubic structures with ordered vacancies and empty spheres were put in place of the missing nitrogen/carbon atoms. However, the assumed positions of the vacancies are not given. The relaxation of the Ti atoms was neglected. The peak positions of the calculated LMTO DOS of $Ti_4N_2\square_2$ agree well with those of the FLAPW DOS of δ'-Ti_2N. However, in the case of the LMTO calculation, the N s and N p peaks are broader and the pseudogap between the N p and the Ti d peak is less pronounced. Also, the Fermi level is situated at a small peak of the DOS and not in a gap. If the DOS calculated by different methods were comparable, this would indicate that δ'-Ti_2N is stabilized with respect to cubic $Ti_4N_2\square_2$ by its special arrangement of vacancies and the relaxation of the Ti atoms.

In order to calculate the valence XPS spectrum of δ'-Ti_2N, the partial local DOS were weighted by energy- and l-dependent photoabsorption cross sections and then superposed [28]. The calculated spectrum was broadened with a spectrometer function of half-width 1.2 eV [27] in order to simulate the finite resolution of the spectrometer. Finally, lifetime broadening was introduced by folding the calculated spectrum with a Lorentzian of half-width $\delta = 0.35$ eV. The photoabsorption cross sections were determined by means of a multiple-scattering formalism where the final state of the emitted photoelectron is described by a LEED function [28]. In agreement with Redinger *et al* [28], the Ti s and p cross sections are found to be very large. Therefore, Ti s and p states contribute significantly to the calculated spectrum although the corresponding partial local DOS are only small components of the density of states. A contribution of similar order of magnitude comes only from the N s states.

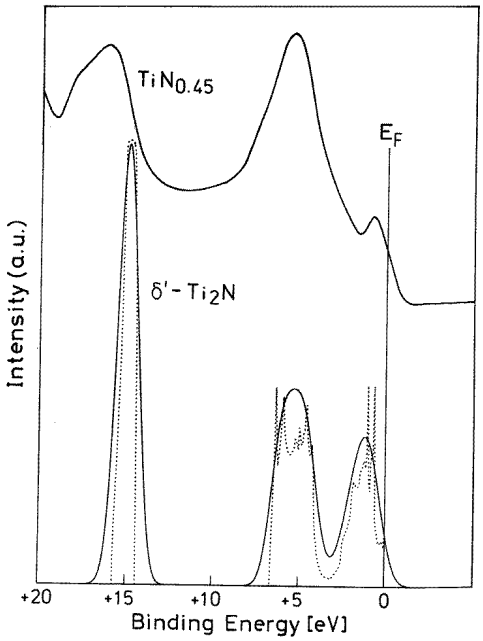

Figure 13. Calculated unbroadened (dotted curve) and broadened (solid curve) valence XPS spectra of δ'-Ti_2N (below) and the measured valence XPS spectrum of δ-$TiN_{0.45}$ [27] (above) in arbitrary units. The binding energy is given with reference to the Fermi level as energy zero. For the broadened spectrum, spectrometer broadening ($S = 1.2$ eV) and lifetime broadening ($W = 0.35$ eV) were taken into account.

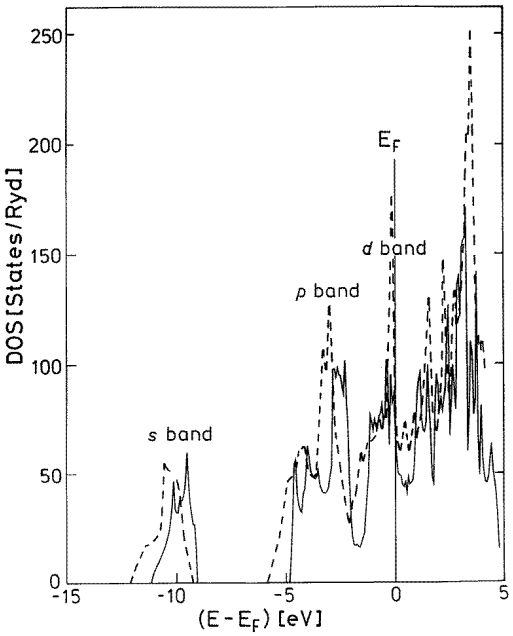

Figure 14. The density of states of fictitious δ'-Ti_2C. The same units as in figure 7 are used. Dotted curve: the tight-binding LMTO DOS for $Ti_4C_2\square_2$ [31].

Figure 13 compares the calculated XPS spectrum of δ'-Ti_2N with the measured spectrum of δ-$TiN_{0.45}$ [27]. The sample of this composition was shown to consist of a mixture of a solid α-Ti(N) solution and of δ-TiN [29], not of metastable δ'-Ti_2N. One can speculate though that the change of structure would only lead to small energy shifts which cannot be detected in the spectra because of the large spectrometer broadening of half-width 1.2 eV. The measured spectrum still contains some background intensity. Taking all of this into consideration, the agreement between the measured and calculated spectra is good. The calculated peak positions are situated at slightly lower binding energies than are found by experiment and the deviations increase with the binding energy of the electrons. Also, the calculated intensity of the peak just below the Fermi level is too high compared with experiment. Similar deviations between measured and calculated valence XPS spectra have been previously reported for titanium nitrides and are commonly ascribed to shortcomings of density functional theory [28].

3.3. Electron densities

The electron density of a solid is obtained by summing up the contributions of all occupied eigenstates. It is an integral quantity and thus not very sensitive to changes of the band structure. Indeed, a comparison of the LAPW electron-density plots of [15] and of the corresponding plots of the present full-potential calculation shows no significant differences. As an example, the FLAPW p- and d-band electron densities of δ'-Ti_2N in the (010) plane are presented in the figures 16(b) and 17(b), later. All of the conclusions of [15] derived from the LAPW electron densities remain valid.

3.4. Comparison of the electronic structures of δ'-Ti_2N and fictitious δ'-Ti_2C

Ti_2C is experimentally found to crystallize not in the δ'-Ti_2N structure but in either the $Fd3m$ or the $R\bar{3}m$ structure which are indistinguishable in powder neutron diffraction. X-ray diffraction of single crystals TiC_x ($x = 0.58$, 0.63 and 0.67) after long thermal treatment showed that the latter phase was the stable phase and the former the metastable phase above 700 K [30]. The coordination of the Ti atoms to the three nearest non-metal vacancies differs for the nitride and the carbide: for δ'-Ti_2N, the vacancies are found in the x-, $-x$- and z-directions with respect to the Ti atom at the origin of a Cartesian coordinate system; for the carbide structures, the vacancies are situated in the x-, y- and z-directions.

In order to find an explanation for the instability of δ'-Ti_2C, FLAPW band-structure calculations were undertaken for (fictitious) δ'-Ti_2C. Its lattice parameters ($a = 8.0016$ au, $c = 16.939\,715$ au) were estimated by multiplying the experimental lattice parameters of δ'-Ti_2N with the ratio of the experimental lattice parameters of cubic TiC and TiN.

Figure 14 shows the DOS of fictitious δ'-Ti_2C. The comparison with the DOS of δ'-Ti_2N shows that, in the carbide, the non-metal s and p bands are shifted to lower binding energies. In the carbide with one valence electron less than for the nitride, the Fermi level lies in an unfavourable position, namely just at the peak at the bottom of the d band. For comparison, the DOS of ordered $Ti_4C_2\square_2$ calculated by means of the tight-binding LMTO method is also shown (dotted curve) [31]. The differences between the LMTO and the FLAPW DOS are more pronounced for the carbide than for the nitride. Owing to tails at the bottom of the two bands, the bands are wider in the case of the LMTO band-structure calculation. The shift of the LMTO non-metal s and p bands to higher binding energies is also more pronounced for the carbide.

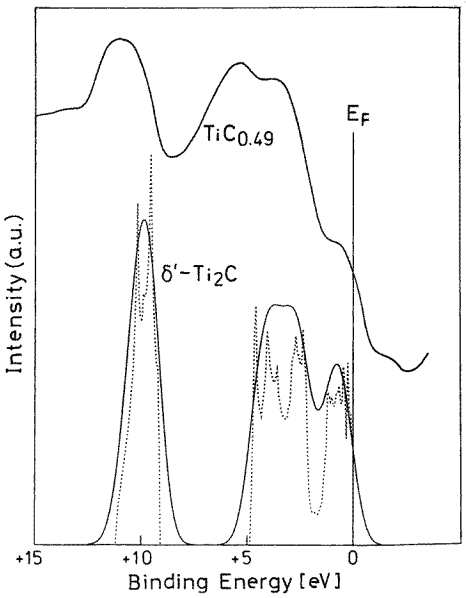

Figure 15. Calculated unbroadened (dotted curve) and broadened (solid curve) valence XPS spectra of fictitious δ'-Ti_2C (below) and the measured valence XPS spectrum of δ-$TiC_{0.49}$ [31] (above) in arbitrary units. The binding energy is given with reference to the Fermi level as energy zero. For the broadened spectrum, only spectrometer broadening ($S = 1.2$ eV) was taken into account.

Figure 15 compares the measured XPS spectrum of $TiC_{0.49}$ [31] with the calculated unbroadened (dotted curve) and broadened (solid curve) XPS spectra of fictitious δ'-Ti_2C. Only spectrometer broadening ($S = 1.2$ eV [31]) was taken into account. Again, the calculated high N s, Ti s and Ti p photoabsorption cross sections cause an increase of intensity for the C s peak and the two peaks at the bottom of the C p band. The calculated C s and C p peaks are shifted to lower binding energies in the calculation compared to experiment and, as in the nitride, the intensity of the peak near the Fermi level is overestimated. Moreover, in the carbide, the calculated p bandwidth of 2 eV is much narrower than the experimental one of 4.5 eV and the two p-band subpeaks are found at a distance of 1 instead of 2 eV. Thus, as already ascertained by Guemmaz *et al* [27, 31], when comparing their calculated LMTO DOS with the measured XPS spectra, the calculated spectrum of the carbide shows more deviations from experiment than that of the nitride. One should not forget, however, that δ'-Ti_2C is a hypothetical phase not yet found by experiment.

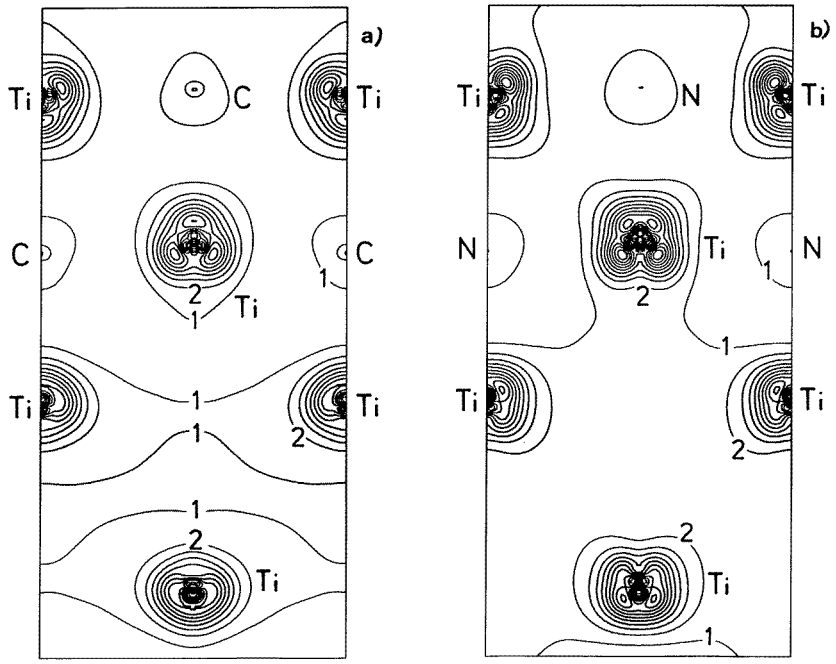

Figure 16. (010) sections of the d-band valence electron densities of (a) (fictitious) δ'-Ti_2C and (b) δ'-Ti_2N. Contour lines on a linear mesh in units of 0.1 e Å^{-3}.

In [15] it was shown that the δ'-Ti_2N structure in the (010) plane looks like a set of ribbons consisting of rows of Ti_2N units, whereas these ribbons are only connected by weak d–d σ-bonds between the Ti atoms octahedrally surrounding the non-metal vacancies. In figure 16, inspection of the d-band electron-density contour plots of δ'-Ti_2N and δ'-Ti_2C in the (010) plane shows that, for the carbide, these bonds do not exist, because the corresponding electronic states are situated above E_F. Hence, the particular arrangement of the non-metal vacancies in the δ'-structure is not as favourable for the carbide as for the nitride. The corresponding p-band electron-density contour plots (figure 17) reveal—as expected—stronger nearest-neighbour p–d σ-bonds for the carbide than for the nitride.

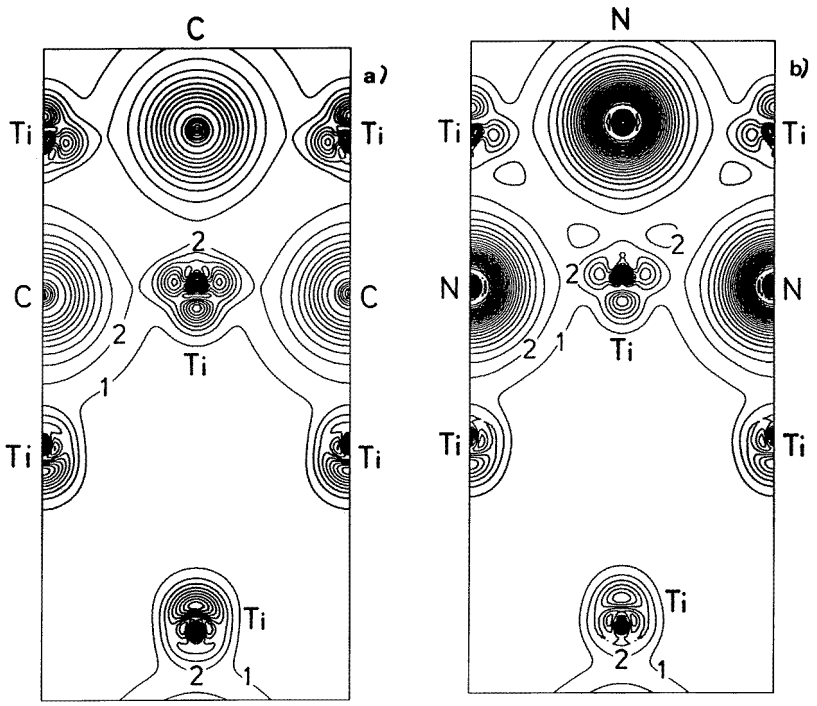

Figure 17. (010) sections of the p-band valence electron densities of (a) (fictitious) δ'-Ti_2C and (b) δ'-Ti_2N. Contour lines on a linear mesh in units of 0.1 e Å^{-3}.

4. Conclusions

(1) Significant differences between the LAPW and FLAPW band structures and densities of states of the two nitrides, ϵ-Ti_2N and δ'-Ti_2N, underline the importance of using a full potential for band-structure calculations of systems with delocalized valence states and an anisotropic charge distribution in the interstitial region.

(2) In accordance with experiment, the ϵ-phase is found to be more stable than the δ'-phase by 9 kJ mol^{-1} because of the stronger Ti–Ti d–d bonds in the former compound which shift the states at the bottom of the d band to lower energies than in δ'-Ti_2N.

(3) In agreement with the neutron diffraction data of Christensen *et al* [9], the δ'-phase is stabilized by the relaxation of the Ti atoms in the z-direction towards the nearest N neighbours. The energy gain by relaxation of 29 kJ mol^{-1} is very large. A shift of the Ti atoms in the other direction (towards the vacancies, as deduced by Nagakura and Kusunoki [8] from XPS spectra) increases the total energy and is therefore not to be expected.

(4) The instability of the δ'-Ti_2N structure for Ti_2C can be qualitatively explained by the position of the Fermi level in a DOS maximum and by the non-existence of d–d σ-bonds between the Ti atoms octahedrally surrounding the vacancies in the carbide.

Acknowledgments

All of the calculations were performed at the Vienna University Computer Centre. Thanks are due to E Umlauf for calculating the electronic structure of fictitious δ'-Ti_2C. I also

want to thank A Neckel and W Wolf for stimulating discussions and valuable comments and suggestions. The financial support of the *Hochschuljubiläumsstiftung der Stadt Wien* (Project H-00111/93) is acknowledged gratefully.

References

[1] Zeng K and Schmid-Fetzer R 1996 *Z. Metallk.* **87** 540
[2] Jonsson S 1996 *Z. Metallk.* **87** 691
[3] Molarius J M, Korhonen A S and Ristolainen E O 1985 *J. Vac. Sci. Technol.* A **3** 2419
[4] Poulek V, Musil J, Valvoda V and Cerny R 1988 *J. Phys. D: Appl. Phys.* **21** 1657
[5] Wriedt H A and Murray J L 1987 *Bull. Alloy Phase Diagrams* **8** 378
[6] Ehrlich P 1953 *Z. Anorg. Chem.* **259** 1
[7] Lobier G and Marcon J P 1969 *C. R. Acad. Sci., Paris* C **268** 1132
[8] Nagakura S and Kusunoki T 1977 *J. Appl. Phys.* **10** 52
[9] Christensen A N, Alamo A and Landesman J P 1985 *Acta Crystallogr.* C **41** 1009
[10] Lengauer W and Ettmayer P 1987 *High Temp.–High Pressures* **19** 673
[11] Etchessahar E, Sohn Y-U, Harmelin M and Debuigne J 1991 *J. Less-Common Met.* **167** 261
[12] Holmberg B 1962 *Acta Chem. Scand.* **16** 1255
[13] Zhou X, Dong H K, Li H D and Liu B 1988 *J. Appl. Phys.* **63** 4942
[14] Lengauer W and Ettmayer P 1986 *J. Less-Common Met.* **120** 153
[15] Eibler R 1993 *J. Phys.: Condens. Matter* **5** 5261
[16] Andersen O K 1975 *Phys. Rev.* B **12** 3060
[17] Koelling D D and Arbman G O 1975 *J. Phys. F: Met. Phys.* **5** 2041
[18] Wimmer E, Krakauer H, Weinert M and Freeman A 1981 *Phys. Rev.* B **24** 864
Jansen H and Freeman A J 1984 *Phys. Rev.* **30** 561
[19] Zhang Z, Shen Y, Xu W and Huang M 1997 *Chin. Phys. Lett.* **14** 542
[20] Herzig P, Redinger J, Eibler R and Neckel A 1987 *J. Solid State Chem.* **70** 281
[21] Hohenberg P and Kohn W 1964 *Phys. Rev.* B **136** 864
[22] Hedin L and Lundqvist S 1972 *J. Physique Coll.* **33** C3 73
[23] Lehmann G and Taut M 1972 *Phys. Status Solidi* **54** 469
[24] Jepsen O and Andersen O K 1971 *Solid State Commun.* **9** 1763
[25] Birch F 1978 *J. Geophys. Res.* **83** 1257
[26] Wolf W 1996 *Thesis* University of Vienna, p 50ff
[27] Guemmaz M, Moraitis G, Mosser A, Khan M A and Parlebas J C 1997 *J. Phys.: Condens. Matter* **9** 8453
[28] Redinger J, Marksteiner P and Weinberger P 1986 *Z. Phys.* B **63** 321
[29] Guemmaz H, Mosser A and Grob J J 1997 *Appl. Phys.* A **64** 407
[30] de Novion C H, Beuneu B, Priem T, Lorenzelli N and Finel A 1990 *The Physics and Chemistry of Carbides, Nitrides and Borides (NATO ASI Series E, vol 185)* ed R Freer (Dordrecht: Kluwer) p 329
[31] Guemmaz M, Moraitis G, Mosser A, Khan M A and Parlebas J C 1997 *J. Electron Spectrosc. Relat. Phenom.* **83** 173